A Multicellular Model of the Renal Myogenic Response

Maria-Veronica Ciocanel[a,*], Tracy L. Stepien[b,c], Ioannis Sgouralis[d], Anita T. Layton[e,*]

[a] *Division of Applied Mathematics, Brown University, Providence, RI, United States*
[b] *School of Mathematical and Statistical Sciences, Arizona State University, Tempe, AZ, United States*
[c] *Present Address: Department of Mathematics, University of Arizona, Tucson, AZ, United States*
[d] *National Institute for Mathematical and Biological Synthesis, University of Tennessee, Knoxville, TN, United States*
[e] *Department of Mathematics, Duke University, Durham, NC, United States*

Abstract

One of the key autoregulatory mechanisms that controls blood flow in the kidney is the myogenic response. Subject to elevated blood pressure, the renal afferent arteriole responds with an increase in muscle tone and a decrease in diameter. We investigate the myogenic response of a vascular segment of multiple smooth muscle cells by connecting instances of afferent arteriole cell models in series. To model individual cells, we include detailed Ca^{2+} signaling, transmembrane transport of major ions, the kinetics of myosin light chain phosphorylation, as well as cellular contraction and wall mechanics. The cells of the vessel are connected by gap junctions, which link the cytoplasm of neighboring cells, and by a layer of endothelial cells. Blood flow through the afferent arteriole vessel is modeled using Poiseuille flow. Simulation of an inflow pressure up-step leads to vasoconstriction in the proximal part of the vessel and to vasodilation for a down-step. The afferent arteriole model stabilizes to a significant degree a physiological range of blood pressures (80–180 mmHg) and predicts a decrease in the average segment diameter for high blood pressures. Similar responses are also observed for short-term pressure pulses. The developed model allows for the study of the effect of oscillatory perturbations to inflow pressure on the

*Corresponding author
Email addresses: alayton@math.duke.edu (Anita T. Layton)

blood flow. The ability of the model to represent the myogenic response suggests that it can be incorporated as a key component into models of integrated renal hemodynamic regulation.

Key words: smooth muscle, gap junctions, microcirculation, kidney, hemodynamics, non-linear model

2010 MSC: 92C30, 92C35

---

1. Introduction

The kidneys are organs in the body of mammals that extract waste from blood and regulate the balance of water, electrolytes, acid-base species, etc. [1]. The kidneys accomplish these crucial tasks by filtering blood through the nephrons where a portion of the supplied blood is extracted from the bloodstream. As the extracted fluid flows through the nephrons, its composition constantly changes, as water and solutes are selectively reabsorbed or secreted, depending on the organism's homeostatic status.

To maintain proper kidney functions, the rate of filtration into each of the nephrons must be maintained within a narrow range [1]. If the filtration rate is high, the kidney may not have sufficient capacity to reabsorb all that is needed and necessary substances may be lost in urine. If the filtration rate is low, the kidney may reabsorb more than is needed and unnecessary substances or toxic waste may leak back into the general circulation. To regulate filtration rate, blood flow in the nephron is controlled by a number of *autoregulatory mechanisms* [2, 3, 4, 5], all of which share a common effector, namely the suppling blood vessel, called *afferent arteriole*.

One of the key mechanisms acting on the afferent arteriole is the *myogenic response* [6]. This mechanism induces vasoconstriction of the arteriole when blood pressure is elevated and vasodilation when blood pressure is reduced. This way the myogenic response enables the kidney to actively impede or accelerate blood flow and therefore to adjust the filtration rate in response to perturbations of blood pressure.

At the vascular level, the myogenic response has been well characterized experimentally and theoretically, for example [7, 8, 9, 10]. However, at the cellular level little is known about the involved phenomena [5]. A goal of this study is to gain a better understanding of the involved intercellular interactions. To that end, we expand on a previously published, highly detailed mathematical model of Ca^{2+} signaling within an afferent arteriole smooth muscle cell [11]. That model represents the transmembrane transport of major ions, intracellular Ca^{2+} dynamics, the kinetics of myosin light chain phosphorylation, and the mechanical behavior of the cell. Here we extend a multi-cell vascular model of the afferent arteriole presented with blood flow, initially developed in [12], that adopts the cellular model of [11], by incorporating a layer of endothelial cells, and we use the resulting model to study the myogenic response of the afferent arteriole at the cellular and vascular level.

2. Mathematical Model

In this section we describe the model equations, the numerical methods developed for the solution of the model equations, and present values for the model parameters.

2.1. Model Description

In our model of the afferent arteriole, we couple individual smooth muscle cells through gap junctions, the endothelium, and blood flow.

2.1.1. Vascular Blood Flow

To obtain an accurate representation of blood flow we model a segment of the renal vasculature consisting of an afferent and the associated efferent arterioles as shown in Fig. 1. We represent the two vessels as consecutive straight tubes that extend from the cortical radial artery ($x = 0$) to the glomerulus ($x = L_{\mathrm{AA}}$), and from the glomerulus to the entrance of the peritubular capillary network ($x = L_{\mathrm{AA}} + L_{\mathrm{EA}}$), respectively.

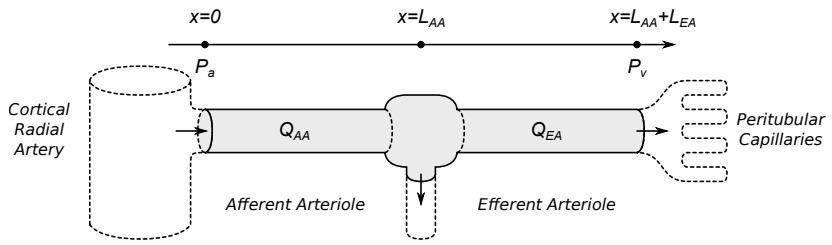

Figure 1: Model vasculature. Blood flows through the *afferent arteriole* from the cortical radial artery to the glomerulus and subsequently flows through the *efferent arteriole* from the glomerulus to the peritubular capillaries.

Let Q_{AA} and Q_{EA} denote the blood flow in the model afferent and efferent arterioles, respectively. In the glomerulus, a portion of the supplied blood is removed from the bloodstream due to filtration [1]. To model glomerular filtration, we assume a constant filtration fraction f_{g}. So, the single nephron glomerular filtration rate equals $f_{\mathrm{g}}Q_{\mathrm{AA}}$ and conservation of mass reads

$$Q_{\mathrm{EA}} = (1 - f_{\mathrm{g}})Q_{\mathrm{AA}}. \tag{1}$$

Blood flow in the model vasculature is assumed to obey Poiseuille's law [13], which, applied to the two vessels, reads

$$\frac{\partial P}{\partial x} = -\frac{8\mu}{\pi R^4}Q_{\mathrm{AA}}, \qquad 0 < x < L_{\mathrm{AA}}, \tag{2}$$

$$\frac{\partial P}{\partial x} = -\frac{8\mu}{\pi R^4}Q_{\mathrm{EA}}, \qquad L_{\mathrm{AA}} < x < L_{\mathrm{AA}} + L_{\mathrm{EA}}. \tag{3}$$

In the above equations, P and R denote the pressure and radius profiles along the model vasculature, respectively, and μ denotes the blood viscosity, which is assumed equal in both vessels (see Fig. 1). Micro-puncture studies indicate minor pressure differences between the renal artery and the entrance of the afferent arteriole, as well as between the peritubular capillaries and the renal

vein [14, 15]. Therefore, we use the boundary conditions

$$P(t,0) = P_{\mathrm{a}}, \tag{4}$$

$$P(t, L_{\mathrm{AA}} + L_{\mathrm{EA}}) = P_{\mathrm{v}}, \tag{5}$$

where P_{a} and P_{v} denote the blood pressures in the renal artery and vein, respectively. As in previous modeling studies [16, 17, 9], we assume P_{a} is a prescribed function of time, while P_{v} is fixed. To facilitate the presentation in Section 3, we refer to the pressures $P_{\mathrm{AA}}(t,0)$ and $P_{\mathrm{AA}}(t, L_{\mathrm{AA}})$ as afferent arteriole *inflow* and *outflow* pressures, respectively.

Conservation of mass (1), Poiseuille's law (2)–(3), and the boundary conditions (4)–(5) can be combined to yield

$$Q_{\mathrm{AA}} = \frac{P_{\mathrm{a}} - P_{\mathrm{v}}}{W_{\mathrm{AA}} + W_{\mathrm{EA}}}, \tag{6}$$

where the vascular resistances W_{AA} and W_{EA} are given by

$$W_{\mathrm{AA}} = \frac{8\mu}{\pi} \int_0^{L_{\mathrm{AA}}} \frac{1}{R^4} dx, \tag{7}$$

$$W_{\mathrm{EA}} = (1 - f_{\mathrm{g}}) \frac{8\mu}{\pi} \int_{L_{\mathrm{AA}}}^{L_{\mathrm{AA}} + L_{\mathrm{EA}}} \frac{1}{R^4} dx. \tag{8}$$

Autoregulatory phenomena in the renal vasculature typically require 1–60 seconds to develop [2, 3, 4]. On this time scale, the radius of the efferent arteriole appears essentially constant [4], therefore for $x > L_{\mathrm{AA}}$ we assume $R(t,x) = R_{\mathrm{EA}}$, where R_{EA} is a fixed radius. So (8) reduces to

$$W_{\mathrm{EA}} = \frac{8(1 - f_{\mathrm{g}})\mu L_{\mathrm{EA}}}{\pi R_{\mathrm{EA}}^4}. \tag{9}$$

In contrast, over the same time scale, the radius of the afferent arteriole may change considerably due to either spontaneous contractions of the arteriolar smooth muscles or the operation of the autoregulatory mechanisms [6, 9]. Therefore, to accurately predict the evolution of $R(t,x)$ for $x < L_{\mathrm{AA}}$, we develop a detailed model of the afferent arteriolar wall that is described below.

2.1.2. Coupling Vascular Smooth Muscle Cells

The wall model consists of a chain of N_{AA} smooth muscle cells oriented circumferentially along the afferent arteriole as shown in Fig. 2. The muscle

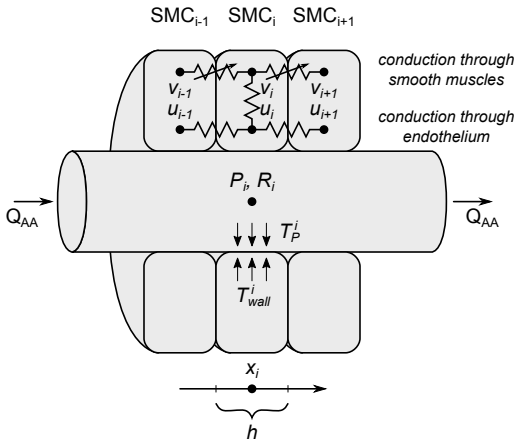

Figure 2: A segment of the model afferent arteriole. The vascular wall consists of a chain of smooth muscle cells (SMC). The local vascular radius R_i is determined by the balance of T_P^i and T_{wall}^i which depend on local blood pressure P_i and the contractile state of the surrounding smooth muscle, respectively. Along the vascular wall, signals are conducted directly through the smooth muscles ($v_{i-1} \leftrightarrow v_i \leftrightarrow v_{i+1}$) or indirectly through the endothelium ($u_{i-1} \leftrightarrow u_i \leftrightarrow u_{i+1}$).

cells are located at

$$x_i = \left(i - \frac{1}{2}\right) h, \qquad i = 1, \ldots, N_{\text{AA}}, \tag{10}$$

where $h = L_{\text{AA}}/N_{\text{AA}}$ is the axial muscle width.

For each smooth muscle cell we adopt the model of [11] which represents detailed transmembrane ionic transport, Ca^{2+} dynamics, and kinetics of myosin light chain phosphorylation. Among other variables, the smooth muscle cell model predicts muscle membrane potential v_i, cytosolic concentrations $[k]_i$ for $k = K^+$, Na^+, Cl^-, Ca^{2+}, and the fraction ψ_i of phosphorylated myosin light chains. In [11] the muscles are studied in isolation, so the developed model does not account for signals shared between different smooth muscles [18]. In the present study we extend the model of [11] by the addition of gap junctional coupling motivated by the model of [12]. To represent gap junctions, we model two pathways: a direct one where ions pass between the cytosol of adjacent

smooth muscles, and an indirect one where electrical currents pass between the smooth muscles and the endothelium [19]. For the former, we compute the ionic fluxes according to the Goldman-Hodgkin-Katz equation similar to [20]. For the latter, we assume each smooth muscle is associated with an endothelial compartment with local membrane potential u_i, and compute the electrical fluxes according to Ohm's law similar to [21]. In summary, the modified muscle dynamics are given by

$$C_{\mathrm{m}} \frac{dv_i}{dt} = -I^i_{\mathrm{net}}(P_i) - I^i_{\mathrm{m}\leftrightarrow\mathrm{m}} - I^i_{\mathrm{m}\leftrightarrow\mathrm{e}}, \tag{11}$$

$$\mathrm{V}_{\mathrm{cyt}} \frac{d[k]_i}{dt} = J^i_{\mathrm{net},k}(P_i) + J^i_{\mathrm{m}\leftrightarrow\mathrm{m},k}, \tag{12}$$

for $k = \mathrm{K}^+$, Na^+, Cl^-, Ca^{2+} and the potential dynamics of the endothelial nodes u_i are given by

$$C_{\mathrm{e}} \frac{du_i}{dt} = I^i_{\mathrm{m}\leftrightarrow\mathrm{e}} - I^i_{\mathrm{e}\leftrightarrow\mathrm{e}}. \tag{13}$$

Above, C_{m} and C_{e} denote the capacitances of the smooth muscle membrane and the endothelial compartments, respectively; $\mathrm{V}_{\mathrm{cyt}}$ denotes the volume of the muscle cytosol; $I^i_{\mathrm{net}}(P_i)$ denotes the net sum of the currents passing through membrane channels [11]; $I^i_{\mathrm{m}\leftrightarrow\mathrm{m}}$, $I^i_{\mathrm{e}\leftrightarrow\mathrm{e}}$, and $I^i_{\mathrm{m}\leftrightarrow\mathrm{e}}$ denote the currents passing through gap junctions developed between muscles and the endothelium [20, 21]; and $J^i_{\mathrm{net},k}$ and $J^i_{\mathrm{m}\leftrightarrow\mathrm{m},k}$ denote the corresponding ion fluxes [11, 20]. For the above equations, we assume no-flux boundary conditions at both end points of the afferent arteriole. Notice that the model muscle cells represent the *myogenic response* according to which the afferent arteriole responds to changes in blood pressure [6]. For this, the model incorporates in $I^i_{\mathrm{net}}(P_i)$ and $J^i_{\mathrm{net,k}}(P_i)$ contributions from pressure sensitive membrane channels whose activation depends on local blood pressure

$$P_i(t) = P(t, x_i), \qquad i = 1, \ldots, N_{\mathrm{AA}}, \tag{14}$$

where $P(t, x)$ is the pressure profile of (2).

We denote the fraction of myosin light chains that are phosphorylated by ψ_i and refer to [11, 12] for its dependence on the model variables. Given ψ_i

and pressure P_i, the model of [11] predicts the local vascular radius R_i in the vicinity of the i^{th} smooth muscle. In particular, R_i is determined by the balance of hoop stresses T_P^i and T_{wall}^i that are exerted across the muscle,

$$\eta \frac{dR_i}{dt} = T_P^i(P_i, R_i) - \xi_i T_{\text{wall}}^i(\psi_i, R_i). \tag{15}$$

The Laplace stress T_P^i depends on P_i and tends to stretch the smooth muscle, causing passive vasodilation. The wall stress T_{wall}^i depends on ψ_i and tends to compress the muscle, causing active vasoconstriction [11]. As the pressure P_i decreases along the vessel [16], the stress T_P^i is lower near the glomerulus than near the cortical radial artery. To achieve a baseline radius profile that is approximately flat, we introduce a parameter ξ_i in (15) which downscales T_{wall}^i similar to the baseline T_P^i. That is, we set

$$\xi_i = 1 + \left(\frac{P_{\text{g}}^{\text{ref}}}{P_{\text{a}}^{\text{ref}}} - 1 \right) \frac{x_i}{L_{\text{AA}}}, \tag{16}$$

where $P_{\text{a}}^{\text{ref}}$ and $P_{\text{g}}^{\text{ref}}$ denote reference values for the afferent arteriole inflow and outflow pressures.

2.2. Numerical Methods

To obtain solutions of the model equations we need to solve a large system of ordinary differential equations that describes the dynamics of the smooth muscle cells. The system can be put in the form

$$\frac{dX_i}{dt} = F_i(X_{i-1}, X_i, X_{i+1}, P_i), \qquad i = 1, \ldots, N_{\text{AA}}, \tag{17}$$

where X_i combines the state variables of the i^{th} smooth muscle cell (for example X_i combines v_i, u_i, $[k]_i$, ψ_i, R_i, etc.). We implement no-flux boundary conditions assuming $X_0 = X_1$ and $X_{N_{\text{AA}}+1} = X_{N_{\text{AA}}}$. The system in (17) is coupled to the blood flow representation of Section 2.1.1, which is discretized spatially. For this we assume that the radius profile is locally approximated by the smooth muscle predictions

$$R(t, x_i) = R_i(t), \qquad i = 1, \ldots, N_{\text{AA}}. \tag{18}$$

Given (6), (7), and (8), blood flow in the afferent arteriole is computed by

$$Q_{\mathrm{AA}} = \frac{\pi}{8\mu} \frac{P_{\mathrm{a}} - P_{\mathrm{v}}}{\sum_i \frac{h}{R_i^4} + (1 - f_{\mathrm{g}}) \frac{L_{\mathrm{EA}}}{R_{\mathrm{EA}}^4}}. \tag{19}$$

Pressures at the discrete locations P_i are obtained via (2) using an upwind approximation of the gradient $\partial P/\partial x$. Namely, the pressures are given by

$$P_1 = P_{\mathrm{a}} - \frac{4\mu h}{\pi} \frac{Q_{\mathrm{AA}}}{R_1^4}, \tag{20}$$

$$P_{i+1} = P_i - \frac{4\mu h}{\pi} \left(\frac{1}{R_{i-1}^4} + \frac{1}{R_i^4} \right) Q_{\mathrm{AA}}, \qquad i = 2, \ldots, N_{\mathrm{AA}}. \tag{21}$$

To compute numerical solutions we cast the resulting system of semi-discrete equations (17), (19), (20), and (21) in the form

$$\frac{dY}{dt} = G_1(t, Y, Z), \tag{22}$$

$$0 = G_2(t, Y, Z), \tag{23}$$

where $Y = (X_1, \ldots, X_{N_{\mathrm{AA}}})$ and $Z = (Q_{\mathrm{AA}}, P_1, \ldots, P_{N_{\mathrm{AA}}})$. For the time evolution of (22)–(23) we apply standard numerical methods for initial value problems in differential-algebraic form [22, 23].

2.3. Parameters

2.3.1. Vascular Geometry and Hemodynamics

Throughout this study, we consider an afferent arteriole of total length $L_{\mathrm{AA}} = 60$ μm that consists of cells with axial length $h = 3$ μm approximately of the same dimensions as reported in [24, 25]. Based on the estimated L_{AA} and h, the model afferent arteriole is discretized into $N_{\mathrm{AA}} = 20$ cells.

Values for the model parameters are listed in Table 1. These are chosen based on previous modeling studies or have been computed assuming reference values for the afferent arteriole inflow and outflow pressures $P_{\mathrm{a}}^{\mathrm{ref}}$ and $P_{\mathrm{g}}^{\mathrm{ref}}$, afferent arteriole radius $R_{\mathrm{AA}}^{\mathrm{ref}}$, afferent arteriole blood flow $Q_{\mathrm{AA}}^{\mathrm{ref}}$, and single nephron glomerular filtration rate $Q_{\mathrm{g}}^{\mathrm{ref}}$. We set the radius of the efferent arteriole R_{EA} to 10% larger than $R_{\mathrm{AA}}^{\mathrm{ref}}$ as reported in [26], and we compute the length of efferent arteriole L_{EA} and blood viscosity μ such that the resulting pressure

Table 1: Model parameters.

Description	Parameter	Value	Units	Reference
Reference afferent arteriole inflow pressure	$P_{\mathrm{a}}^{\mathrm{ref}}$	100	mmHg	[16, 17]
Reference afferent arteriole outflow pressure	$P_{\mathrm{g}}^{\mathrm{ref}}$	50	mmHg	[16, 17]
Reference afferent arteriole radius	$R_{\mathrm{AA}}^{\mathrm{ref}}$	10	μm	[11, 17]
Reference afferent arteriole flow	$Q_{\mathrm{AA}}^{\mathrm{ref}}$	300	nl/min	[16, 17]
Reference glomerular filtration rate	$Q_{\mathrm{g}}^{\mathrm{ref}}$	300	nl/min	[9, 17]
Pressure in renal vein	P_{v}	4	mmHg	[9]
Axial length of smooth muscle cell	h	3	μm	[24]
Number of smooth muscle cells	N_{AA}	20	-	present study
Afferent arteriole length	L_{AA}	60	μm	[24]
Efferent arteriole length	L_{EA}	60	μm	present study
Efferent arteriole radius	R_{EA}	11	μm	[26]
Filtration fraction	f_{g}	0.1	-	[27]
Blood viscosity	μ	6.68	mmHg$\times\mu$s	present study
Muscle contraction time constant	η	1.71	s	[11, 12]

drops along the afferent and efferent arterioles at reference are $P_{\mathrm{a}}^{\mathrm{ref}} - P_{\mathrm{g}}^{\mathrm{ref}}$ and $P_{\mathrm{g}}^{\mathrm{ref}} - P_{\mathrm{v}}$, respectively.

2.3.2. Electrophysiology

Values for the parameters modeling the currents I^i_{net} and ion fluxes $J^i_{\mathrm{net,k}}$ of (11)–(12) are adopted from [11, 12], while values for the parameters modeling $I^i_{\mathrm{m}\leftrightarrow\mathrm{m}}$ and $J^i_{\mathrm{m}\leftrightarrow\mathrm{m,k}}$ are adopted from [20]. For the currents $I^i_{\mathrm{m}\leftrightarrow\mathrm{e}}$ and $I^i_{\mathrm{e}\leftrightarrow\mathrm{e}}$ modeling endothelial gap junctions, we use Ohmic conductances g_{me} and g_{ee}, respectively. We compute these values based on the estimated dimensions of the model afferent arteriole, namely

$$g_{\mathrm{me}} = \frac{A_{\mathrm{me}}}{\rho_{\mathrm{me}}\ell_{\mathrm{me}}}\,, \tag{24}$$

$$g_{\mathrm{ee}} = \frac{A_{\mathrm{ee}}}{\rho_{\mathrm{ee}}\ell_{\mathrm{ee}}}\,, \tag{25}$$

where $A_{\mathrm{me}} = 2\pi h R^{\mathrm{ref}}_{\mathrm{AA}}$ is the contact area between the muscles and the endothelium, $A_{\mathrm{me}} = \pi R^{\mathrm{ref}}_{\mathrm{AA}}\ell_{me}$ is the endothelial cross-section area, ℓ_{me} is half of the afferent arteriole wall thickness, and ℓ_{ee} equals h. For the resistivities ρ_{me} and ρ_{ee} we adopt the values from [28].

3. Model Results

We examine the output of our model when the inflow pressure, denoted $P_{\mathrm{a}}(t)$, is set to a constant value, perturbed by an instantaneous rise or drop, and perturbed by sinusoidal oscillations.

3.1. Spontaneous vasodilation

We first compare our model to the previous models of [11] and [12] by studying the base case situation when the inflow pressure P_{a} is set to a constant value of 100 mmHg. Fig. 3A shows the predicted oscillations for the first cell in the afferent arteriole for the membrane potential v_1. The mean value is -35.96 mV, which, when rounded, is the same value as found in both [11, 12] and which approximates the measured value of -40 mV well [29]. Fig. 3B shows the cytosolic

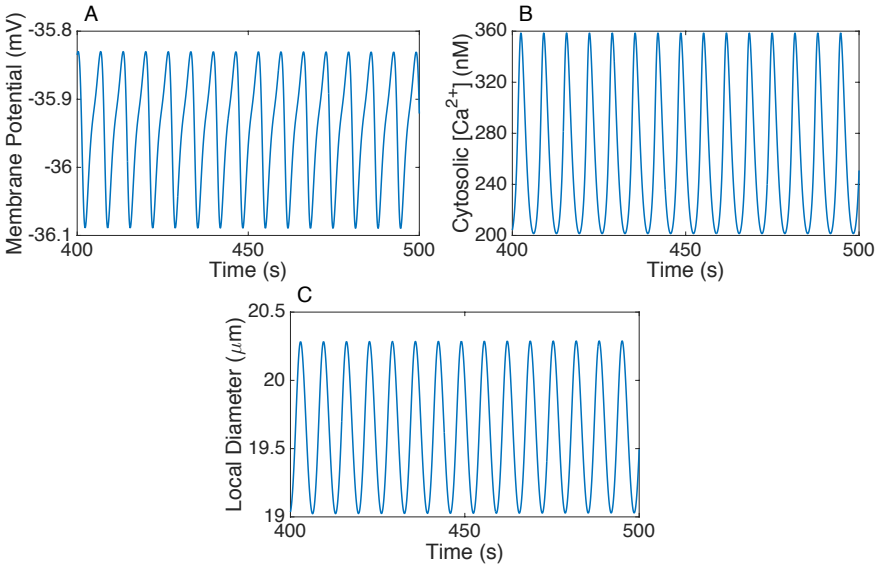

Figure 3: Predicted oscillations for the first cell in the afferent arteriole at an inflow pressure of 100 mmHg for the (A) membrane potential; (B) cytosolic concentration of Ca^{2+}; and (C) afferent arteriole local diameter.

Ca^{2+} concentration, which varies between approximately 200 and 360 nM, a somewhat larger range than as predicted in both [11, 12]. The frequency of the oscillations is 0.15 Hz, the same as in [12] and slightly smaller compared to [11]. This frequency value falls within the range of experimental measurements, for example see [10]. Fig. 3C shows the vascular diameter in the proximity of the first cell of the afferent arteriole, which has an average of 19.7 μm with an oscillation amplitude of 0.6 μm. Both values are in agreement with previous model predictions [11] and also experimental observations of spontaneous vasomotion, for example [26].

To investigate the myogenic response of the model's afferent arteriole, we computed the outflow pressure and time- and space-averaged diameter of the afferent arteriole given different constant inflow pressures P_{a}. As seen in Fig. 4, our results indicate that as P_{a} increases, the outflow pressure of the afferent arteriole increases. The predicted myogenic response lies below the line representing perfect autoregulation (i.e. independence of outflow from inflow pres-

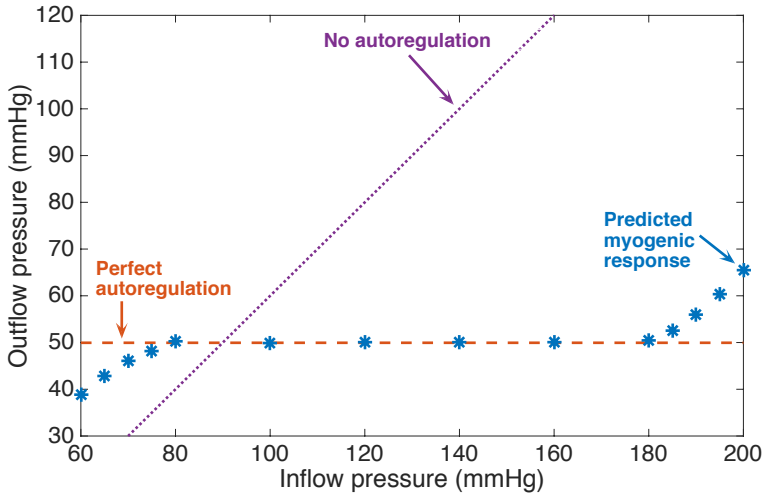

Figure 4: Predicted myogenic response (blue) compared to perfect autoregulation (red) and no autoregulation (purple) of blood flow through the vessel for a range of blood pressures.

sure) for small inflow pressures, coincides with the line for a wide range of inflow pressures (80–180 mmHg), and then lies above the line for large inflow pressures. A similar autoregulatory plateau is predicted for Q_{AA} (not shown). Hence our model is able to achieve almost perfect autoregulation for a larger range of inflow pressures compared to the models of [16, 12]. The blue curve is also significantly different than the slope 1 line representing the case of no autoregulation (purple).

Fig. 5 shows the mean time-averaged diameters across afferent arteriole cells for different constant inflow pressures. As in [16, 12], the model predicts vasodilation for small inflow pressures and vasoconstriction for large inflow pressures. Our model predicts a larger mean diameter for small inflow pressures ($\leq$ 80 mmHg) than [16, 12] and approximately the same mean diameter for large inflow pressures ($\geq$ 160 mmHg).

3.2. Responses to a Step Perturbation

To gain insights into the behavior of the model under time dependent pressure perturbations we simulate changes in inflow pressure as illustrated in Fig. 6,

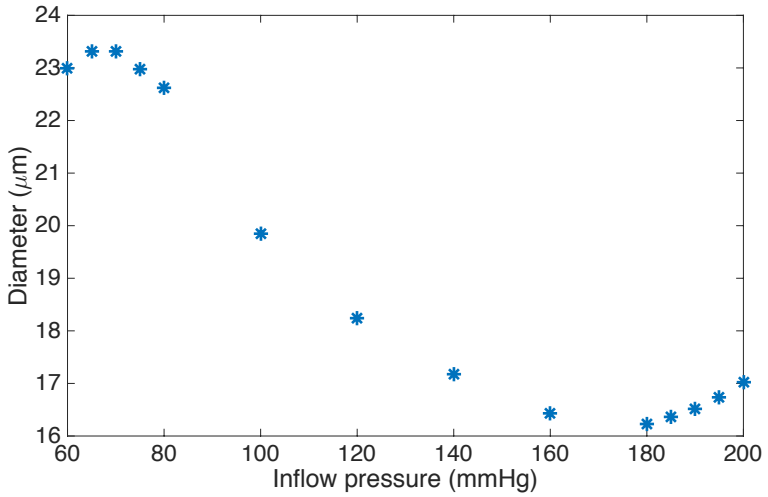

Figure 5: Predicted space- and time-averaged diameters across the afferent arteriole cells for a range of time independent blood pressures.

first row. We simulate a pressure pulse by introducing an almost instantaneous rise (respectively drop) in inflow pressure, maintaining the pulse pressure for 20 seconds, and returning back to the baseline through an almost instantaneous drop (respectively rise). The system is then allowed to stabilize after the return to the baseline inflow pressure over a period of 50 seconds. This framework allows us to analyze the predicted responses of the model afferent arteriole over a short-term period for both increases and decreases in blood pressure and is intended to simulate step-pressure experimental conditions [30].

Rows 2–5 of Fig. 6 show the evolution of flow Q_{AA}, membrane potential, cytosolic Ca^{2+} concentration, and diameter for the first cell in the modeled afferent arteriole under a pressure pulse decrease to 80 mmHg (left) and a pressure pulse increase to 120 mmHg (right). The pressure decrease leads to a reduction in membrane potential, which triggers a rapid decrease in the amplitude of the Ca^{2+} concentration oscillations and subsequently a slower drop in the cell diameter [11, 12]. This reduction in the cell diameter corresponds to passive constriction of the model afferent arteriole due to the sudden pressure drop, which is followed by a slower dilation due to the activation of the myogenic

response (see Fig. 6, A5) [11]. The short pressure pulse does not allow the diameter of the cell to fully dilate to a diameter larger than the baseline 20.1 μm during the pressure decrease. However, the diameter of the cell returns to a larger mean amplitude of oscillations after the return to baseline pressure at 40 s that stabilizes slowly ($\gg$40 s) to the pre-step value.

In the pressure pulse increase, pressure-activated Ca^{2+} and Na^{+} membrane channels open up, allowing the influx of cations, which in turn lead to an increase in membrane potential, as well as cytosolic Ca^{2+} concentration [11, 12]. Following the initial passive dilation, this triggers a rapid active constriction (see Fig. 6, B4, at 20 s). The short pulse period does not allow us to visualize complete constriction in the case of this pressure up-step.

To investigate the propagation of the pressure pulses (Fig. 6, first row) throughout the length of the model afferent arteriole, we show the time evolution of membrane potential, cytosolic Ca^{2+} concentration, and diameter of 5 different cells located throughout the length of the model vessel during a pressure pulse increase to 140 mmHg in Fig. 7. As a result of including the gap junctions (see Section 2.1.2), the membrane potential profiles are similar for all cells. On the other hand, the Ca^{2+} concentration amplitude oscillations after the pulse show that the distal cells (cells spanning the terminal $\sim$20% of the afferent arteriole) differ considerably from their neighbors. The Ca^{2+} fluctuations further affect the local muscle dynamics, so that the diameters of the last model afferent arteriole cells also illustrate larger differences from the proximal and middle cells.

Fig. 8 further illustrates the effect of the myogenic response on the outflow diameter and pressure for the short pulse simulations. Fig. 8A corresponds to the time- and space- averaged (across all cells) diameter of the afferent arteriole. These predictions show that some vasodilation at small inflow pressure pulses and vasoconstriction at large inflow pressure pulses are observed even when investigating short-term responses to pressure changes. Fig. 8B shows that a similar behavior is observed for the time-averaged diameter of the last cell in the model afferent arteriole, as predicted in [16] as well. We note that the

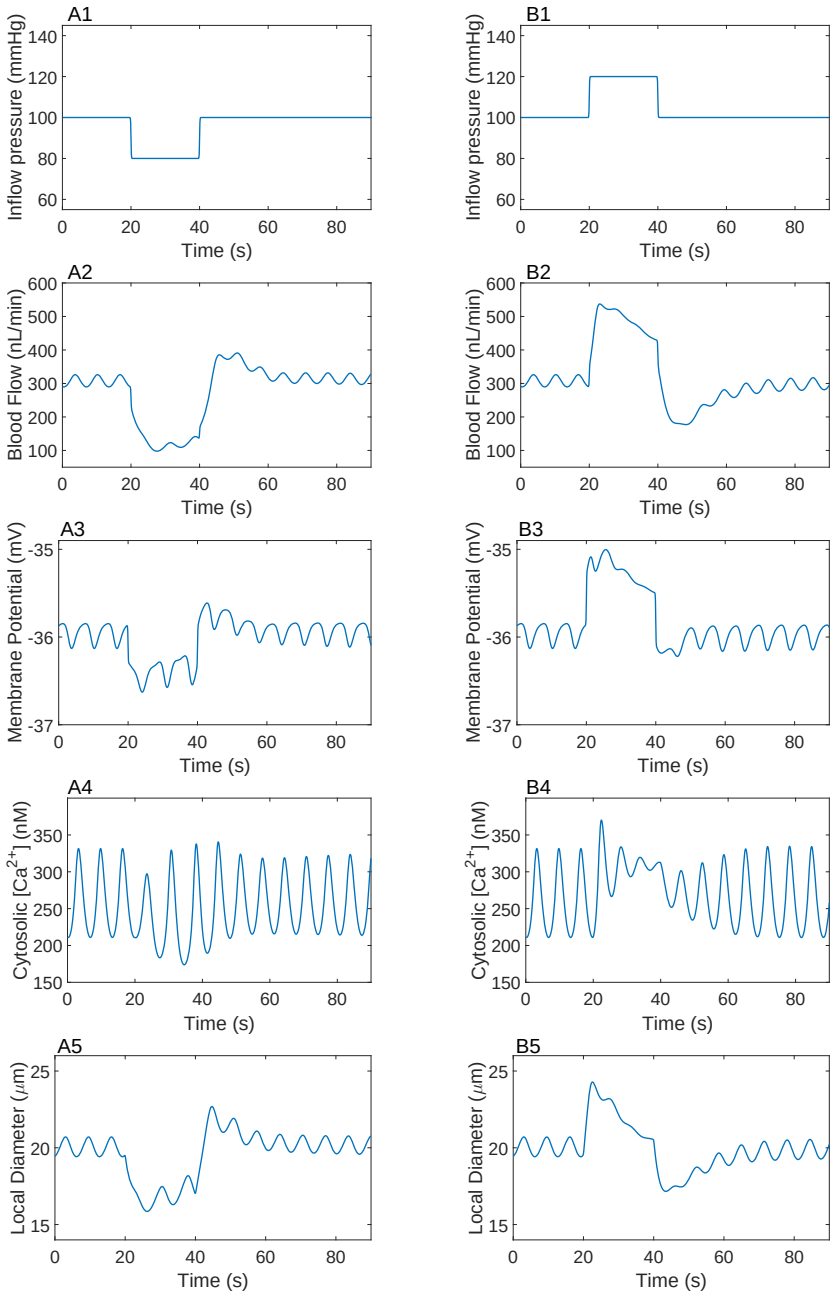

Figure 6: Predicted time profiles of (1) inflow pressure; (2) blood flow; (3) membrane potential; (4) cytosolic Ca^{2+} concentration; and (5) local diameter for the first cell in the model afferent arteriole under (A) pressure pulse decrease to 80 mmHg; and (B) pressure pulse increase to 120 mmHg.

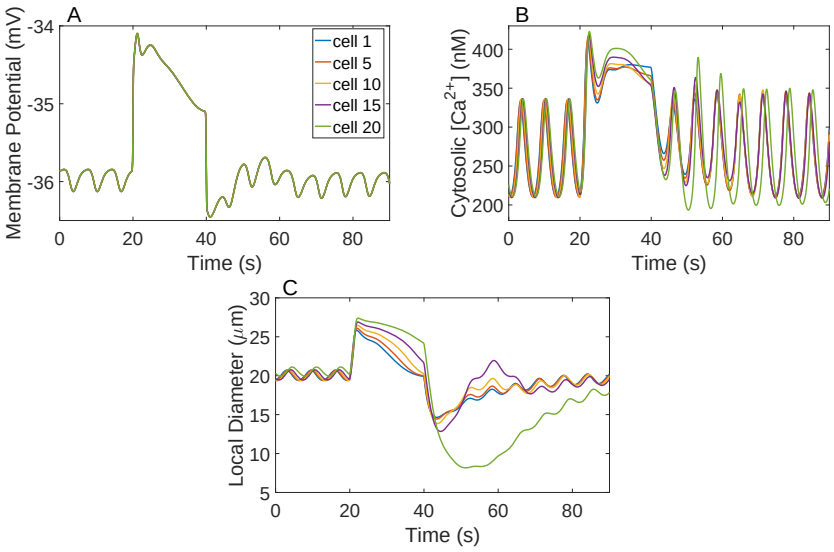

Figure 7: Predicted time profiles of (A) membrane potential; (B) cytosolic Ca^{2+} concentration; and (C) diameter for five cells in the afferent arteriole at an inflow pressure pulse increase to 140 mmHg.

curves in Fig. 8 would be considerably smoother if long-term, fully stabilized responses to pressure pulses were considered instead. These results show that the autoregulation curve behavior is conserved even when considering short-term model afferent arteriole responses.

3.3. Responses to Sinusoidal Perturbation

We next examined the model afferent arteriole's behavior under sinusoidal perturbations in the inflow pressure $P_{\mathrm{a}}(t)$. After setting the inflow pressure to a constant value of $P_{\mathrm{a}}^{\mathrm{ref}}$ for $t < 0$, we perturb the inflow pressure in the form

$$P_{\mathrm{a}}(t) = P_{\mathrm{a}}^{\mathrm{ref}} + A\sin(2\pi f t), \qquad t \geq 0 \tag{26}$$

where A is the amplitude of the sinusoidal inflow pressure and f is the frequency. We studied the model's response to the perturbations for amplitudes $A = 10$ mmHg and $A = 20$ mmHg and for a range of frequencies between 0.01 Hz (slower) and 1 Hz (faster).

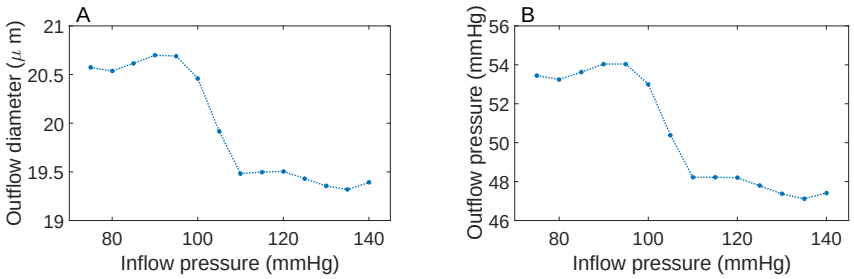

Figure 8: Predicted (A) space- and time-averaged diameter (across all cells); and (B) time-averaged outflow pressure (for the last afferent arteriole cell), for a range of luminal pressure pulses.

For each inflow amplitude A and frequency f, we observe that the oscillations in the outflow pressure contain two or more different frequencies. Three such examples are given in Fig. 9, where the first row shows the perturbed inflow pressure, the second row shows oscillations in the afferent arteriole cell diameters, and the third row shows the resulting outflow pressure. To facilitate the comparison between the induced $P_{\mathrm{a}}(t)$ and predicted $Q_{\mathrm{AA}}(t)$ perturbations we normalize the corresponding time courses by their respective baseline values and combine them in Fig. 10.

The outflow pressure curves (Fig. 9, third row) show that there is a "faster oscillation" with a larger frequency as well as a "slower oscillation" with a smaller frequency. The faster oscillation has approximately the same frequency as the inflow frequency f, and the slower oscillation increases and then plateaus for $f \geq 0.5$ Hz around the value of approximately 0.15 Hz (for both amplitudes $A = 10$ mmHg and $A = 20$ mmHg), which is the natural frequency of the afferent arteriole spontaneous vasomotion reported in Section 3.1.

The amplitude of the outflow pressure is larger than the inflow amplitude A for small frequencies and decreases as the inflow frequency f increases. When the inflow frequency f is greater than or equal to 0.25 Hz, for $A = 10$ mmHg, the outflow amplitude converges to approximately 7.8 mmHg, and for $A = 20$ mmHg, the outflow amplitude converges to approximately 13.5 mmHg. Thus, for smaller inflow frequencies f, the sinusoidal perturbation leads to irregular

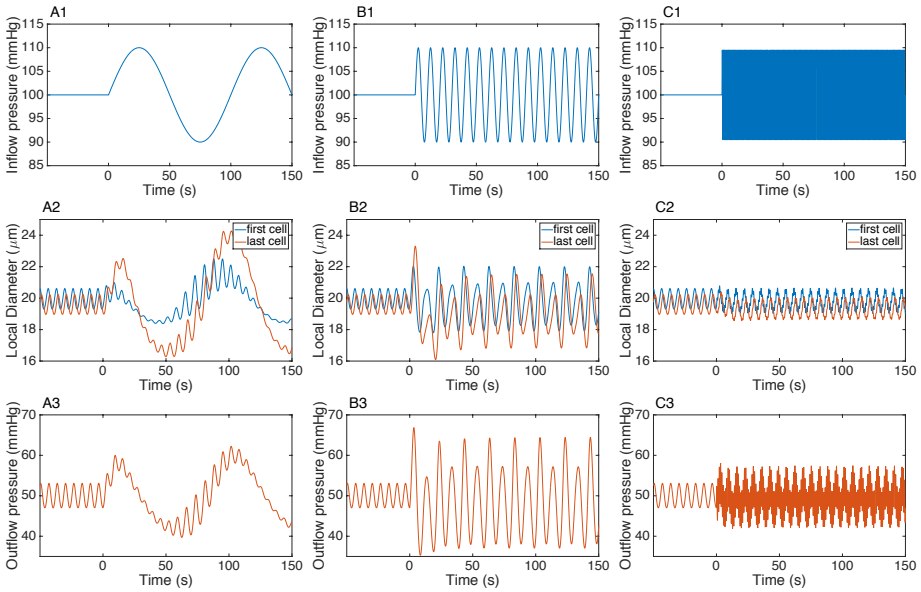

Figure 9: (1) Inflow luminal pressure; and predicted oscillations in (2) local diameter for the first and last cells in the afferent arteriole; and (3) outflow pressure when a sinusoidal perturbation is applied to the inflow pressure with amplitude $A = 10$ mmHg and frequency (A) 0.01 Hz; (B) 0.1 Hz; and (C) 1 Hz.

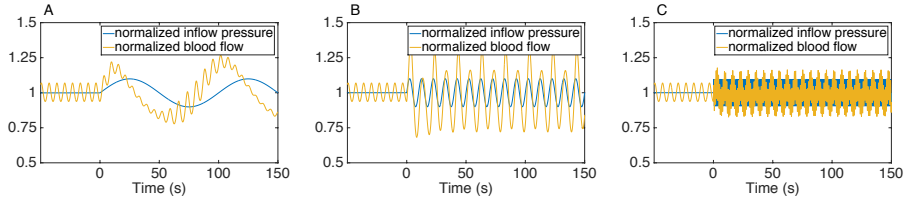

Figure 10: Normalized inflow pressure $P_{\mathrm{a}}/P_{\mathrm{a}}^{\mathrm{ref}}$ and normalized blood flow $Q_{\mathrm{AA}}/Q_{\mathrm{AA}}^{\mathrm{ref}}$ when a sinusoidal perturbation is applied to the inflow pressure with amplitude $A = 10$ mmHg and frequency (A) 0.01 Hz; (B) 0.1 Hz; and (C) 1 Hz.

oscillations in the afferent arteriole cell diameters and outflow pressure, and for large inflow frequencies f, the perturbation leads to sustained vasoconstriction [6, 16, 7, 8].

Assuming that the afferent arteriole behaved like a rigid tube, a linear relationship between P_{a} and Q_{AA} is expected. To see this, we note that (7) reduces to a constant resistance W_{AA}, and therefore (6) implies the linear dependence. For example, under the assumption of a rigid afferent arteriole, a 10% increase of inflow pressure P_{a}, as in Figs. 9 and 10, would result in a 10% increase of Q_{AA} and the sinusoidal oscillations in P_{a} and Q_{AA} would be in phase. However, the afferent arteriole is not a rigid tube, so our simulations indicate a nonlinear relationship between these variables. We find that, similar to the outflow pressure amplitude, the amplitude of the normalized blood flow $Q_{\mathrm{AA}}/Q_{\mathrm{AA}}^{\mathrm{ref}}$ decreases as the inflow frequency f increases and plateaus to approximately 0.17 for $A = 10$ mmHg and approximately 0.29 for $A = 20$ mmHg. Thus, a 10% increase in inflow pressure results in a 17% increase in blood flow rate, and a 20% increase in inflow pressure results in a 29% increase in blood flow rate. For small input frequencies f, Q_{AA} has a phase shift in front of P_{a}, but as f increases, Q_{AA} is shifted after P_{a}.

4. Discussion

We have developed a mathematical model of the afferent arteriole of the rat kidney. The model represents detailed Ca^{2+} trafficking in each of the afferent arteriole smooth muscle cells, as well as the kinetics of myosin light chain phosphorylation, the mechanical behavior of the cell, and vascular blood flow. The multi-cell afferent arteriole model is an extension of our preliminary arteriolar model [12], which does not include conduction via the endothelial layer. As of that, the model in [12] might underestimate the effects of conducted myogenic responses [19] and the impact on the overall autoregulatory behavior of the model vessel [16].

The afferent arteriole segment model of the present study was constructed by

connecting N_{AA} afferent arteriole smooth muscle cell models and N_{AA} endothelial compartments in series. Intercellular coupling allows the representation of ions diffusion and electric conduction along the afferent arteriole. Further, a fluid dynamics model was included to relate fluid pressure, fluid flow, and vascular resistance so as to allow accurate prediction of all variables required for the activation of the myogenic response.

At physiological blood pressures, the model predicts spontaneous oscillations in cytosolic $[Ca^{2+}]$ and in vascular diameter. Those oscillations arise from the dynamic exchange of Ca^{2+} between the cytosol and the sarcoplasmic reticulum, coupled to the stimulation of Ca^{2+}-activated potassium and chloride channels, and the modulation of voltage-activated L-type channels [12, 11]. These spontaneous oscillations of the afferent arteriole muscle tone result in oscillations in vascular resistance, fluid pressure, and flow [9].

By a mechanism known as the *myogenic response*, the afferent arteriole regulates renal blood flow: it reacts to an elevation in blood pressure with an increase in muscle tone and a decrease in luminal diameter. The purpose of the myogenic response is believed to be the stabilization of glomerular filtration and the protection of the vulnerable glomerular capillaries from barotrauma arising from exceedingly high systolic blood pressure, especially in hypertension [31]. The model represents the myogenic response by assuming that the response is initiated by pressure-activated Ca^{2+} and Na^{+} membrane channels [11]. Through its myogenic response, the model afferent arteriole is able to stabilize, to a significant degree, outflow pressure for a range of steady-state inflow pressure, from 80 to 180 mmHg (see Fig. 4).

The afferent arteriole model described here reproduces the myogenic response even when considering short-term pulses in the inflow pressure. Differences in the distal cells in the model vessel are observed, and may be explained by the fluctuations in Ca^{2+} due to the pressure pulses. Sinusoidal perturbations in the inflow pressure are also investigated, and the responses are found to depend on the amplitude and frequency of the perturbation. Since the afferent arteriole is not a rigid tube, the effect of different amplitude oscillations are

found to influence both the increase in the blood flow rate and the phase shift between inflow pressure and flow rate.

Another contributing mechanism in renal hemodynamic control, besides the myogenic response, is the tubuloglomerular feedback mechanism. In tubuloglomerular feedback, the afferent arteriolar muscle tone, and thus blood flow and glomerular filtration rate, is adjusted based on salt reabsorption by the downstream nephron. A useful extension of the present afferent arteriole segment model would be to include a model of nephron transport (e.g., [32, 33]) and tubuloglomerular feedback (e.g., [34, 9]). That would result in an integrative model of renal hemodynamics regulation model that can be used for studying the interactions between the myogenic and tubuloglomerular feedback mechanisms in the context of renal autoregulation, and for investigating changes in renal hemodynamics in pathophysiological conditions, especially under circumstances (e.g., diabetes and hypertension) involving complex cellular responses [5].

Acknowledgements

This work is the product of a workshop and short-term visits supported by the National Institute for Mathematical and Biological Synthesis, an Institute sponsored by the National Science Foundation through NSF Award #DBI-1300426, with additional support from The University of Tennessee, Knoxville. Support was also provided by the National Institutes of Health: National Institute of Diabetes and Digestive and Kidney Diseases and by the National Science Foundation, via grants #DK089066 and #DMS-1263995 to AT Layton.

References

References

[1] J. E. Hall, Guyton and Hall Textbook of Medical Physiology, Elsevier Health Sciences, 2015.

[2] W. A. Cupples, B. Braam, Assessment of renal autoregulation, Am. J. Physiol. Renal Physiol. 292 (2007) F1105–F1123. doi:10.1152/ajprenal.00194.2006.

[3] N. H. Holstein-Rathlou, D. J. Marsh, Renal blood flow regulation and arterial pressure fluctuations: A case study in nonlinear dynamics, Physiol. Rev. 74 (1994) 637–681.

[4] A. Just, W. J. Arendshorst, Dynamics and contribution of mechanisms mediating renal blood flow autoregulation, Am. J. Physiol. Regul. Integr. Comp. Physiol. 285 (2003) R619–R631. doi:10.1152/ajpregu.00766.2002.

[5] M. Carlström, C. S. Wilcox, W. J. Arendshorst, Renal autoregulation in health and disease, Physiol. Rev. 95 (2) (2015) 405–511. doi:10.1152/physrev.00042.2012.

[6] J. Chen, I. Sgouralis, L. C. Moore, H. E. Layton, A. T. Layton, A mathematical model of the myogenic response to systolic pressure in the afferent arteriole, Am. J. Physiol. Renal Physiol. 300 (2011) F669–F681. doi:10.1152/ajprenal.00382.2010.

[7] R. Loutzenhiser, A. Bidani, L. Chilton, Renal myogenic response: Kinetic attributes and physiological role., Circ. Res. 90 (2002) 1316–1324. doi:10.1161/01.RES.0000024262.11534.18.

[8] R. Loutzenhiser, A. K. Bidani, X. Wang, Systolic pressure and the myogenic response of the renal afferent arteriole., Acta Physiol. Scand. 181 (2004) 407–413. doi:10.1111/j.1365-201X.2004.01312.x.

[9] I. Sgouralis, A. T. Layton, Theoretical assessment of renal autoregulatory mechanisms, Am. J. Physiol. Renal Physiol. 306 (2014) F1357–F1371. doi:10.1152/ajprenal.00649.2013.

[10] I. Sgouralis, V. Maroulas, A. T. Layton, Transfer function analysis of dynamic blood flow control in the rat kidney, Bull. Math. Biol. 78 (5) (2016) 923–960. doi:10.1007/s11538-016-0168-y.

[11] A. Edwards, A. Layton, Calcium dynamics underlying the afferent arteriole myogenic response, Am. J. Physiol. Renal Physiol. 306 (2014) F34–F48. doi:10.1152/ajprenal.00317.2013.

[12] V. Ciocanel, T. L. Stepien, A. Edwards, A. T. Layton, Modeling autoregulation of the afferent arteriole of the rat kidney, To appear in AWM Proceedings for NIMBioS WS for Women in Mathematical Biology.

[13] I. Sgouralis, A. T. Layton, Mathematical modeling of renal hemodynamics in physiology and pathophysiology, Math. Biosci. 264 (2015) 8–20. doi:10.1016/j.mbs.2015.02.016.

[14] B. M. Brenner, J. L. Troy, T. M. Daugharty, Pressures in cortical structures of the rat kidney, Am. J. Physiol. 222 (1972) 246–251.

[15] P. P. Leyssac, Further studies on oscillating tubulo-glomerular feedback responses in the rat kidney, Acta Physiol. Scand. 126 (1986) 271–277. doi:10.1111/j.1748-1716.1986.tb07814.x.

[16] I. Sgouralis, A. Layton, Autoregulation and conduction of vasomotor responses in a mathematical model of the rat afferent arteriole, Am. J. Physiol. Renal Physiol. 303 (2012) F229–F239. doi:10.1152/ajprenal.00589.2011.

[17] I. Sgouralis, A. T. Layton, Control and modulation of fluid flow in the rat kidney, Bull. Math. Biol. 75 (2013) 2551–2574. doi:10.1007/s11538-013-9907-5.

[18] P. R. Brink, Gap junctions in vascular smooth muscle, Acta Physiol. Scand. 164 (1998) 349–356. doi:10.1046/j.1365-201X.1998.00439.x.

[19] D. Casellas, P. K. Carmines, Control of the renal microcirculation: Cellular and integrative perspectives, Curr. Opin. Nephrol. Hypertens. 5 (1996) 57–63.

[20] A. Kapela, A. Bezerianos, N. M. Tsoukias, A mathematical model of vasoreactivity in rat mesenteric arterioles: I. Myoendothelial communication, Microcirculation 16 (2009) 694–713. doi:10.3109/10739680903177539.

[21] I. Sgouralis, A. T. Layton, Conduction of feedback-mediated signal in a computational model of coupled nephrons, Math. Med. Biol. 33 (2015) 87–106. doi:10.1093/imammb/dqv005.

[22] L. F. Shampine, M. W. Reichelt, The MATLAB ODE Suite, SIAM J. Sci. Comput. 18 (1997) 1–22. doi:10.1137/S1064827594276424.

[23] K. E. Brenan, S. L. Campbell, L. R. Petzold, Numerical Solution of Initial-Value Problems in Differential-Algebraic Equations, Vol. 14, Society for Industrial and Applied Mathematics, Philadelphia, PA, 1996.

[24] L. Chilton, K. Loutzenhiser, E. Morales, J. Breaks, G. J. Kargacin, R. Loutzenhiser, Inward rectifier K(+) currents and Kir2.1 expression in renal afferent and efferent arterioles, J. Am. Soc. Nephrol. 19 (1) (2008) 69–76. doi:10.1681/ASN.2007010039.

[25] K. Loutzenhiser, R. Loutzenhiser, Angiotensin II-induced Ca(2+) influx in renal afferent and efferent arterioles: differing roles of voltage-gated and store-operated Ca(2+) entry, Circ. Res. 87 (7) (2000) 551–557. doi:10.1161/01.RES.87.7.551.

[26] D. Casellas, L. C. Moore, Autoregulation and tubuloglomerular feedback in juxtamedullary glomerular arterioles, Am. J. Physiol. 258 (3) (1990) F660–F669.

[27] S. C. Thomson, R. C. Blantz, Biophysics of glomerular filtration, Compr. Physiol. 2 (3) (2012) 1671–1699. doi:10.1002/cphy.c100089.

[28] H. K. Diep, E. J. Vigmond, S. S. Segal, D. G. Welsh, Defining electrical communication in skeletal muscle resistance arteries: a computational approach, J. Physiol. 568 (1) (2005) 267–281. doi:10.1113/jphysiol.2005.090233.

[29] R. Loutzenhiser, L. Chilton, G. Trottier, Membrane potential measurements in renal afferent and efferent arterioles: Actions of angiotensin II, Am. J. Physiol. Renal Physiol. 273 (1997) F307–F314.

[30] A. K. Bidani, R. Hacioglu, I. Abu-Amarah, G. A. Williamson, R. Loutzenhiser, K. A. Griffin, "Step" vs. "dynamic" autoregulation: implications for susceptibility to hypertensive injury, Am. J. Physiol. Renal Physiol. 285 (1) (2003) F113–F120. doi:10.1152/ajprenal.00012.2003.

[31] R. Loutzenhiser, K. Griffin, G. Williamson, A. Bidani, Renal autoregulation: new perspectives regarding the protective and regulatory roles of the underlying mechanisms, Am. J. Physiol. Regul. Integr. Comp. Physiol. 290 (5) (2006) R1153–R1167. doi:10.1152/ajpregu.00402.2005.

[32] A. Layton, V. Vallon, A. Edwards, Modeling oxygen consumption in the proximal tubule: effects of NHE and SGLT2 inhibition, Am. J. Physiol. Renal Physiol. 308 (12) (2015) F1343–F1357. doi:10.1152/ajprenal.00007.2015.

[33] A. Layton, V. Vallon, A. Edwards, Predicted Consequences of diabetes and SGLT inhibition on transport and oxygen consumption along a rat nephron, Am. J. Physiol. Renal Physiol. 310 (2016) F1269–F1283. doi:10.1152/ajprenal.00543.2015.

[34] A. Layton, Feedback-mediated dynamics in a model of a compliant thick ascending limb, Math. Biosci. 228 (2010) 185–194. doi:10.1016/j.mbs.2010.10.002.